AUTOMATIC REGISTRATION FOR WIDE FIELD IMAGER (WFI) L4 IMAGERY TIME SERIES

Marina Ferreira[1], *Daniel Braga*[1], *Ezequiel Rocha*[1], *Ítalo Mira*[1], *Alisson Cleiton de Oliveira*[1], *Gilberto Ribeiro de Queiroz*[1], *Thales Sehn Körting*[1], *Cláudia Almeida*[1], *Leila Maria Garcia Fonseca*[1]

[1]Earth Observation and Geoinformatics Division (DIOTG). National Institute for Space Research (INPE), São José dos Campos, SP 12227-010 – Brazil, {marina.ferreira; daniel.braga; ezequiel.rocha; italo.rafael; alisson.oliveira; gilberto.queiroz; thales.korting; claudia.almeida; leila.fonseca}@inpe.br

ABSTRACT

The WFI sensor systems on board the CBERS satellite family and Amazonia-1 conduct imaging revisits of the Earth's surface at intervals of approximately five days and thus can support many remote sensing applications. A fundamental data product for such applications is the L4 image processing level corresponding to the image orthorectification. However, WFI time series may present spatial displacements and positional distortions between images from the same location. In the present work, CBERS-4, CBERS-4A and Amazonia-1 imagery time series of Aracaju, in Sergipe State, were analyzed, highlighting the displacement between images due to variations in the registration of each satellite, their respective coordinate projection and spatial resolution. The methodology used in this work consisted of developing an automated code in Python that automatically corrects the aforementioned problems in WFI L4 time series, through the co-registration technique using the library AROSICS. The results showed that images from the same sensor as the reference, presented minor displacements (average of 0,59 pixel) while the ones that required resampling had major displacements (average of 1,17 pixel).

Keywords– *CBERS, AMAZONIA-1, Image Processing, Python, Co-registration.*

1. INTRODUCTION

The use of optical images generated by orbital sensors is essential for monitoring disturbances and changes in the most diverse ecosystems on the Earth's surface [1]. Among the various sensor systems currently applied to these purposes, the Wide Field Imager (WFI) stands out by its temporal resolution of 1-3 days when users combine the joint use of Brazilian satellites.

The WFI sensor is an update to the sensors present on the CBERS-1, 2 and 2B satellites, now incorporated on the CBERS-4, 4A and Amazonia-1 satellites. These sensor systems have significant improvements in their internal parameters compared to previous versions, such as improved geometric and radiometric performances and increased spatial (64 m or 55 m), spectral (four multispectral bands: RGBNir) and temporal (~5 days) resolutions [2, 3]. The innovation brought by this sensor system also consists of its functioning as a complement to other sensors with different temporal resolutions (e.g. AVHRR/NOAA, MODIS/Terra and Aqua or the TM/Landsat) [2]. Furthermore, WFI images when accompanied by the term "L4" refer to the highest level of image processing, when there is orthorectification [4]. Time series of images acquired by WFI sensor allow several environmental process and monitoring of the Brazilian territory.

However, the harmonization of time series by this sensor system faces challenges, such as spatial displacements and positional distortions between images. In the case of the time series analyzed, this shift occurs because, although the WFI sensor settings are similar for the CBERS-4, 4A and Amazonia-1 satellites, they may present variations in their registration and respective coordinate projection. These variations occur due to the influence of the atmosphere, lighting conditions, data acquisition geometry, storage failures and internal sensor parameters [2,5,6]. To overcome these problems, the application of co-registration or automatic registration of WFI L4 images is justified.

Automatic image registration is a technique that aligns different images of a same location acquired at different times, angles and sensors [7], a recurring fact in time series composition. Furthermore, the assessment of displacement after co-registration is crucial for a quantitative analysis of the effectiveness of the process. This helps prevent errors and ensures data accuracy after co-registration, which is vital for applications such as change detection, mosaics, image fusion, among others [8].

Currently, there is a wide variety of software and libraries available to perform the automatic recording of time series, such as ARRSI, COSICorr, AROP and RMSEs. Among these, the Automated and Robust Open Source Image Co-Registration Software (AROSICS) stands out as a viable alternative for this process, due to its generic and operational applicability in various raster image formats and open source [8]. The objective of this work was to automate the recording of time series for the same region using easily applicable and scalable open-source libraries.

2. MATERIAL AND METHODS

2.1. Data acquisition and processing

The data was acquired using the image catalog of the National Institute for Space Research (INPE). We constructed a time series with 24 L4 images from WFI aboard the CBERS-4A, CBERS-4 and Amazonia-1 satellites (8 from Amazonia-1, 6 from CBERS-4A and 10 from CBERS-4), covering the city of Aracaju (Sergipe, Brazil), referring to the months of January and February 2024. For

data processing, as well as the processing of resampling and co-registration, we used the Jupyter Notebook v. 4.0.11 via Anaconda platform v. 3.1.7. Libraries used included Matplotlib, AROSICS, OS, Pandas, Geopandas, GDAL, Numpy, Rasterio, Dbfread, Tabulate and Re, Skimage and Shutil. To run this project was used a machine with 16GB RAM and processor Intel® Core™ i7, 11th generation, with 8 CPUs operating in 2.8GHz.

2.2. CBERS-4A image resampling

Images acquired by the WFI on board the CBERS-4 and Amazonia-1 satellites have different spatial resolutions than the CBERS-4A images, being 64 m and 55 m, respectively. Therefore, before co-registration, it was necessary to resample the images in order to standardize them. This process consists of processing a digital image to change its spatial resolution, adjusting and resizing all individual pixels.

This process was conducted using the nearest neighbor method, which keeps the radiometric pixel original values. This method interpolates the estimated pixel value of CBERS-4A images (from 55 m to 64 m), considering only the value of the closest sample, being chosen for its computational efficiency and for keeping the brightness values of the pixels unchanged during resampling [9,10].

2.3. Reference image for co-registration

One of the main challenges when working with time series images obtained by satellites is the contamination of spectral information by clouds and noise [2]. It is still possible to observe difficulty on the part of modern sensors in effectively penetrating clouds [11], resulting in a significant obstacle in the automatic analysis and recording of time series using optical and infrared bands. During the selection of the reference image for co-register the individual components of our time series, obtained from the smallest occurrence of clouds, a code was developed for identifying cloud areas through the numerical brightness reference. The algorithm counted the values in the image matrix, considering as a cloud the values that exceed a pre-defined threshold, obtaining in return a mask, in which only the brightest pixels are represented in a new image. The cloud mask identifies points of cloud presence and whether their identification was appropriate.

2.4. Co-registration Method

For time series processing that includes image co-registration, evaluating displacement is essential to verify consistency across multiple bands [12]. The AROSICS v. 1.11.0 library was used to carry out the co-registration process. This tool evaluates the correspondence of the analyzed images in the frequency domain, using the Fourier Shift Theorem [8].

The theorem describes the change in phase of the spectrum of a given signal. Taking as a basis a regular grid defined over the image, in which each point can be considered a signal and its frequency response, the spatial displacement of that point is obtained [13]. According to [14], correlation based on phase analysis provides more accurate results compared to spatial correction techniques. This approach has the ability to detect large displacements in images without compromising subpixel accuracy. Aiming to guarantee more cohesive responses in relation to signal intensity comparison, the algorithm was adjusted to apply band-to-band co-registration of the reference image, in relation to the target image based on the definition of some parameters (Figure 1).

Parameters	Description
grid_resolution = 10	Grid resolution in pixels in the x-direction
windows_size = (20)	Size of the moving window
min_reliability = 0	Minimum reliability for co-registered points
align_grids = True	Align the target image grid with the reference

Table 1. Parameters defined for applying AROSICS (adapted from [8]).

Finally, the local co-registration function of the AROSICS library was applied, containing as input parameters of the reference image, target images and the parameters described on Table 1. Nevertheless, displacement corrections were applied to the images according to the calculated information. In this work, only the NIR band was used to evaluate co-registration. This band was chosen given its lower sensitivity to atmospheric effects and its better behavior in co-registration processing, when compared to other optical bands [15,16].

3. RESULTS AND DISCUSSION

3.1. Reference image

After successfully performing resampling, to select the reference image, the comparison involved the image with the highest percentage of cloud coverage and the image with the lowest percentage of cloud.

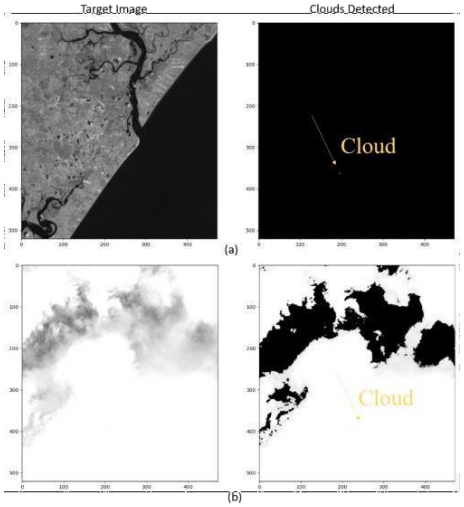


Figure 1. Cloud detection for an image (a) with low presence and (b) with high presence.

Figure 1a presents the image from January 7, 2024 captured by the Amazonia-1 satellite, which recorded the lowest percentage of clouds of all images in the time series,

with only 0.0028%. So this image was used as a reference for the co-registration stage.

3.2. Co-register

Figure 2 presents the result of co-registration of one of the images that comprises the time series analyzed in this work, being an image from the Amazonia-1 satellite and another from CBERS-4.

It should be noted that color compositions have been used in the images to better visualize the differences and to illustrate the effectiveness of the process. Furthermore, Figure 2 presents a difference image to highlight the pixel displacements between images before and after co-registration. Thus, the blue color represents the pixels that were not displaced, indicating a good initial alignment, while the white color highlights the pixels that were displaced during the co-registration process.

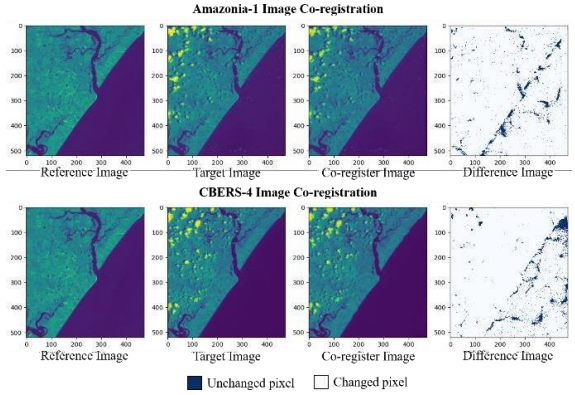


Figura 2. Images from Amazonia-1 and CBERS-4 post co-registration.

3.3. Spatial displacement

Figure 3 provides a visualization of the most significant displacements observed. All images that experienced the largest displacements were identified, indicating possible areas of interest or substantial changes in the object of study. At the same time, areas with smaller displacements were also highlighted, which are crucial for evaluating the stability and reliability of co-registration.

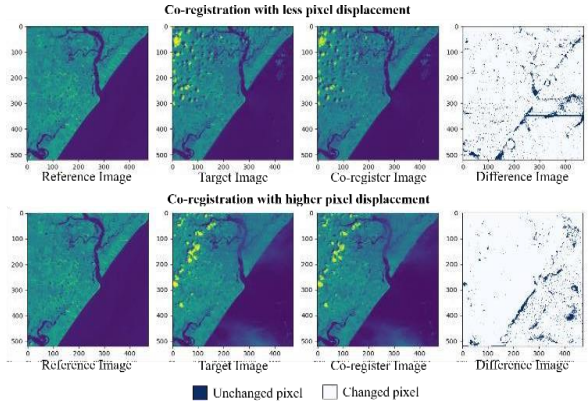


Figure 3. Images with minimum and maximum displacement in pixels after co-registration.

As a way of analyzing the application of the method, an evaluation of the average displacements of the images submitted to the process was carried out, referring to the NIR band. The WFI images were organized in sequence by satellite (following the order: Amazonia-1, CBERS-4A and CBERS-4), excluding the reference image. The Table 2 shows the displacements, in pixel unit, for each image compared with the reference. It was then verified that image 3 from the CBERS-4A satellite (img_3_CB4A) presented the largest average displacement (1,54 pixel) in relation to the reference image. On the other hand, image 1 from the Amazonia-1 satellite (img_1_AMZ) showed the smallest average displacement after co-registration (0,33 pixel), when compared to the reference image.

Image	Minimum Shift (Pixel)	Maximum Shift (Pixel)	Average Shift (Pixel)
IMG_1_AMZ	0.04	6.43	0.34
IMG_2_AMZ	0.03	5.36	0.51
IMG_3_AMZ	0.04	5.95	0.58
IMG_4_AMZ	0.03	6.59	0.55
IMG_5_AMZ	0.01	6.77	0.40
IMG_6_AMZ	0.07	5.09	0.87
IMG_7_AMZ	0.06	6.61	0.85
IMG_1_CB4A	0.11	6.39	1.31
IMG_2_CB4A	0.07	6.37	1.20
IMG_3_CB4A	0.07	6.51	1.54
IMG_4_CB4A	0.09	6.12	0.72
IMG_5_CB4A	0.12	6.14	1.06
IMG_6_CB4A	0.10	6.47	1.16
IMG_1_CB4	0.09	6.97	1.37
IMG_2_CB4	0.09	6.57	0.62
IMG_3_CB4	0.04	6.69	0.55
IMG_4_CB4	0.02	5.43	0.49
IMG_5_CB4	0.05	6.34	1.38
IMG_6_CB4	0.06	6.41	1.01
IMG_7_CB4	0.03	6.94	1.48
IMG_8_CB4	0.05	6.62	1.47
IMG_9_CB4	0.07	6.60	0.86
IMG_10_CB4	0.08	6.81	1.42

Table 2. Displacement of each image compared to the reference image in pixel units.

As shown on Table 2, the shifts from Amazonia-1 images presents in general, smallest values (average of 0.59 pixel), compared to the others. It may be justified by the origin of the reference image, since it belongs to the same sensor. In the other hand, images from CBERS-4A, that were resampled, shows higher shifts values (average of 1.17 pixel). The process of resampling might result on geometric changes, which could be an explanation of the high differences of CBERS-4A images against Amazonia-1 or CBERS-4 images.

4. CONCLUSION

The evaluation of positional distortions is performed to estimate and correct the spatial displacement of each WFI image. This type of geometric inconsistency occurs due to specific changes in the use of WFI on satellites from different missions. For example, although the WFI sensor used in CBERS-4A has similar specifications to the CBERS-4 satellite, its spatial resolution became 55 m at nadir due to the reduction in CBERS 4A's altitude (INPE, 2019). In relation to the Amazonia1 satellite, the same spatial displacement process can be observed during image acquisition, further justifying the need to apply the automatic co-registration technique for WFI images at Level 4.

Co-registration, despite being satisfactorily applied by the developed algorithm, has limitations. For the WFI L4 time series with 24 images, the processing time was around 25 to 30 minutes for all the images. Therefore, for larger time series, in size or number of images, or with smaller correspondence windows, high computational power and long processing times would be required. Another limiting factor is the level of reliability of the points detected for recording. In this algorithm, a reliability value of 0 (min_reliability) was defined, indicating the acceptance of points with at least 40% reliability for registration.

Although this work presents a good approach for dealing with registration issues, future works are needed to increase the reliability of the points to be registered as well as the process of defining the reference image, to make sure that the one selected is the best in terms of georeferencing.

5. ACKNOWLEDGMENTS

To FAPESP (2020/09215-3) and CNPq (311324/2021-5).

6. REFERENCES

[1] LOVELAND, T. R.; DWYER J. L. Landsat: Building a strong future. *Remote Sensing of Environment*, v. 122, pp. 22–29, 2012.

[2] ARANTES et al. Disponibilidade de imagens Landsat-TM para o estudo de séries temporais no Brasil, Anais do XIX Simpósio Brasileiro de Sensoriamento Remoto, v. 19, 2019.

[3] COSTA, C. A. M. et al. Técnicas de processamento de imagens para registro automático: aplicações em PAN/CBERS-4. *Proceedings XXIV GEOINFO*, pp. 485–490, 2023.

[4] OSHIRO, O. T. et al. Monitoramento do desmatamento no bioma amazônico com o satélite Amazonia-1. In: SILVA, L. F. DA; OLIVEIRA, V. C. DE. (org.). Cultivando o futuro: tendências e desafios nas ciências agrárias 2. Ponta Grossa, PR: Atena, pp. 22–31, 2024.

[5] LEONARDI, S. S. et al. Comparação do desempenho de algoritmos de normalização radiométrica de imagens de satélite. *Anais XI SBSR*, Belo Horizonte, Brasil, pp. 2063–2069, 2003.

[6] NETO, H. L. et al. Aplicação de redes neurais recorrentes em séries temporais de estações meteorológicas para imputação de dados: uma abordagem sobre micro estações meteorológicas na região oeste do Pará. *Anais do XI Workshop de Computação Aplicada à Gestão do Meio Ambiente e Recursos Naturais*, pp. 171–180, 2020.

[7] MISRA, I. et al. Phobos image enhancement using unpaired multi-frame acquisitions from Indian Mars Color Camera. *Planetary and Space Science*, v. 201, 2021.

[8] SCHEFFLER, D. et al. Arosics: an automated and robust opensource image co-registration software for multi-sensor satellite data. *Remote Sensing*, v. 9, pp. 676, 2017.

[9] JENSEN, R. J. *Sensoriamento Remoto do Ambiente: Uma perspectiva em Recursos terrestres*. Parêntese, São José dos Campos, SP, Brasil, 1987.

[10] M. E. R BEZERRA. Métodos baseados na regra do vizinho mais próximo para reconhecimento de imagens. *Trabalho de Conclusão de Curso (Bacharel em Engenharia da Computação) - Escola Politécnica de Pernambuco – Universidade de Pernambuco. Recife*, 2006.

[11] MARKHAM, B. L. et al. Landsat sensor performance: history and current status. *IEEE Transactions on Geoscience and Remote Sensing*, v. 42, pp. 2691-2694, 2004.

[12] JHAN, J. P. et al. Investigation of parallax issues for multi-lens multispectral camera band co-registration. *The International Archives of the Photogrammetry, Remote Sensing and Spatial Information Sciences*, v. XLII-2/W6, pp. 4–7, 2017.

[13] BROTOISWORO, P. et al. Automated georeferencing of Diwata-2 multispectral imagery using feature matching. *J. Phys.: Conf. Ser.* v. 2214 , 2022.

[14] T. KONG, L; WANG. Fast image registration based on phase spectrum difference. *Third international conference on instrumentation, measurement, computer, communication and control.*, pp. 1503–1506, 2013.

[15] LEACH, N. et al. Normalization method for multi-sensor high spatial and temporal resolution satellite imagery with radiometric inconsistencies. *Computers and Electronics in Agriculture*, v. 164, 2019.

[16] PÉREZ, A. F. et al. A deep learning approach to satellite image time series coregistration through alignment of road networks. *Neural Computing and Applications*, v. 36, pp. 3583–3593, 2024.